ACS OMEGA

Open Access

http://pubs.acs.org/journal/acsodf

Article

Deciphering the Chemotherapeutic Role of the Aryl Hydrocarbon Receptor Antagonist Resveratrol against the High-Penetrance Genes of Triple-Negative Breast Cancer

Published as part of ACS Omega virtual special issue "3D Structures in Medicinal Chemistry and Chemical Biology".

Prarthana Chatterjee,[†] Rohit Karn,[†] Arnold Emerson. I, and Satarupa Banerjee*

Cite This: *ACS Omega* 2024, 9, 30350−30363

Read Online

ACCESS | Metrics & More | Article Recommendations | Supporting Information

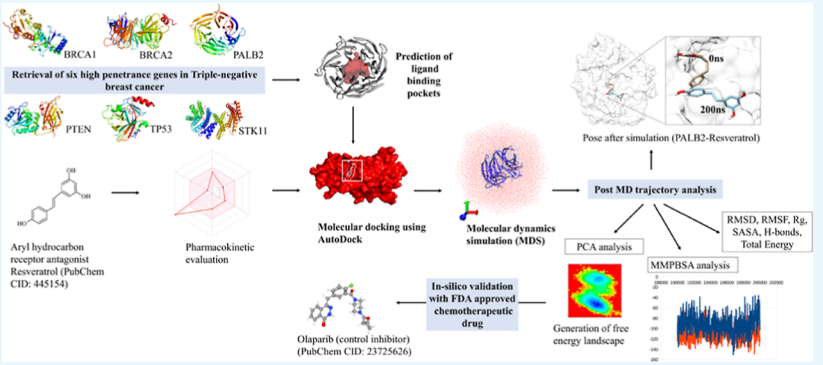

ABSTRACT: In addition to several other malignancies, the ligand-activated aryl hydrocarbon receptor (AhR) signaling pathway has been found to enhance the risk of triple-negative breast cancer (TNBC). Many natural compounds of pharmaceutical importance are identified as antagonistic exogenous ligands of AhR. The expressional lack of hormone receptors coupled with adverse prognosis leads to the absence of molecular-targeted therapy in TNBC. Hence, discovering low-cost therapeutic alternatives involving the identification of effective biomarkers is an urgent necessity. This study investigates the binding mechanism of resveratrol, a dietary exogenous AhR ligand against the high-penetrance genes in TNBC, viz., PALB2, TP53, PTEN, STK11, BRCA1, and BRCA2. Post-pharmacokinetic evaluation, molecular docking revealed the binding energy scores of resveratrol against the six TNBC high-penetrance receptors. The results obtained from docking were confirmed by molecular dynamics simulation including principal component analysis, calculation of total interaction energy, and free-energy landscape computation. PALB2 emerged as a promising therapeutic receptor of resveratrol. Furthermore, the PALB2−resveratrol binding dynamics were evaluated against olaparib, an FDA-approved standardized TNBC inhibitor. Our study reveals comparatively better chemistry of PALB2−resveratrol than PALB2−olaparib. Considering the current surge in the discovery of precision medicine in biomarker-based cancer therapeutics, this study proposes PALB2−resveratrol as a unique drug−receptor combination thus awaiting validation through in vitro studies.

1. INTRODUCTION

Currently, breast cancer (BC) persists as the dominant cause of malignancy-related deaths among women worldwide. It has surpassed lung cancer as the highest and most commonly diagnosed malignancy globally and second in terms of cancer mortality in the US.[1,2] The tremendous molecular variability of BC may be partially attributed to the ambiguity of the three main hormone receptors, viz., estrogen (ER), human epidermal growth factor 2 (HER2), and progesterone (PR).[3−5] Based on the expression profile of the endocrine receptors, hormone-responsive luminal BC, receptor-deprived triple-negative BC (TNBC), and HER2-enriched BC are categorized as the primary subclasses of mammary malignancy. Substantial breakthroughs in clinical oncology have succeeded in reducing the global hormone-receptive BC mortality rate; TNBC is specifically linked to extremely adverse prognosis. As the name suggests, the hormone-refractory TNBC lacks the ER, PR, and HER2 receptor expression and corresponds to about 15−20% of breast carcinomas reported annually. The

Received: February 9, 2024
Revised: June 4, 2024
Accepted: June 7, 2024
Published: July 1, 2024

expression dearth of the related endocrine receptors makes TNBC therapeutics relatively challenging.[6] A majority of over 50% of patients experience a relapse within 3 to 5 years postdiagnosis. The rapid rate of distant metastasis, a significantly shorter overall survival (OS), and subsequent development of multidrug resistance are the characteristic hallmarks of TNBC.[7,8]

Given the emerging scientific evidence that common environmental toxicants including dioxins and dioxin-like compounds play a crucial role in the development of several malignancies, including the various BC subtypes, increased attention is now being paid to the various molecular mechanisms by which pollutants induce tumor formation, invasion, and metastasis. Previously, the majority of studies on environment-induced carcinogenesis focused on the genotoxic chemical's ability to induce mutation, damage DNA, and initiate tumors. Recent research, however, points to additional, nongenotoxic routes comprising cellular receptors, such as the aryl hydrocarbon receptor (AhR) that could be elicited by ligands from the environment.[9] Several investigations have indicated that exposure to chemicals, followed by AhR activation, affects the mammary glands' differentiation mechanism, leading to pregnancy-related concerns and challenges in breastfeeding, eventually raising the risk of BC.[10] Subsequent research has further established the molecular role of AhR in the onset of tumorigenesis, thereby consolidating the participation of AhR in BC promotion and metastasis.[11] The multifaceted nature of ligand-specific AhR signaling is impacted by pharmacokinetic factors, compound-induced AhR conformational deviations, and several other vital parameters.[12] A plethora of endogenous or exogenous ligands can either activate or deactivate the ligand-sensitive AhR-signaling pathway. The majority of these ligands function as AhR antagonists, thus limiting the signaling of activated AhR at the onset of malignancy. Polyphenols including flavonoids, stilbenoids, carotenoids, and indoles are some phytocompounds that comprise the antagonistic dietary exogenous ligands of AhR.[13] The aforementioned natural metabolites are well-known for their pharmaceutical and therapeutic activities, including anticancer, antimicrobial, and antioxidant properties, and enzymatic protein kinase and cytochrome P450 inhibitory activities with minimum therapeutic side effects.[13,14] Resveratrol (*trans*-3,4′,5-trihydroxystilbene) is one such polyphenolic stilbene, which is recognized as a natural AhR antagonist found abundantly in grapes, berries, peanuts, and red wine.[15] It has been demonstrated to be cytotoxic in vitro in a plethora of human malignant cells as in ovary, breast, skin, cervix, colon, prostate, and thyroid carcinomas.[16,17] The antimalignant role of resveratrol is exerted in a multitude of cancer phases from the onset of the tumorigenesis to its progression through the regulation of the several signal-transduction pathways impacting tumor proliferation, metastasis, angiogenesis, and invasion. Neoplasia initiation is associated with spontaneous genetic alteration when subjected to carcinogenic exposure, ultimately leading to mutagenesis. Chemical carcinogens fail to induce DNA damage unless metabolized by the phase-I biotransformative cytochrome P450 enzymes (CYP1A1, CYP1A2, and CYP1B1).[18] Hence inhibiting the irreversible activity of the phase-I enzymes and activity augmentation of the phase-II enzymes is a therapeutic approach for the conversion of chemical carcinogens into soluble and relatively less toxic compounds.

Several reports claim elevated AhR expression to be associated with advanced-stage breast malignancy compared to that in an early stage. Following a prolonged estradiol expression, an abrupt rise in AhR expression was observed in MCF-7 and MCF10AT1 neoplastic breast cell lines with a corresponding receptor suppression of ER and PR.[19] Furthermore, these receptor expression changes were accompanied by apoptosis inhibition, aggressive invasion, and enhanced cellular proliferation. When apoptosis-promoting chemotherapy medications like doxorubicin, paclitaxel, and lapatinib were coadministered with the MDA-MB-231 TNBC cell line pretreated with 2,3,7,8-tetrachlorodibenzo-*p*-dioxin (TCDD), apoptosis inhibition was noted.[20] Reports claim MCF-7 exposure to combinations of polycyclic aromatic hydrocarbons (PAHs) that attach and activate AhR increases the proliferation of malignant cells and boosts antiapoptotic protein secretion by AhR pathway modulation.[21] Resveratrol is also reported to restrict the AhR-induced cytochrome P450 enzyme activity that drives the procarcinogen conversion to carcinogens in response to xenobiotics. In the breast epithelial cell line MCF-10A, resveratrol also inhibited the TCDD-mediated expression and function of cytochrome enzymes CYP1A1 and CYP1B1. Additionally, in BC cell line MCF-7 and HepG2 liver cancer cells, it was found to abrogate benzo[*a*]pyrene (B[*a*]P)-induced CYP1A1 and CYP1A2 activity and impair the upregulated signal transduction of the carcinogen activating enzymes.[22] Thus, resveratrol acts as a blocking agent in the conversion of the inactive procarcinogen into an active carcinogen by inhibiting the aryl hydrocarbon-induced cytochrome P450 enzymatic activities responsible for the liver metabolism of xenobiotics.[23] Goode and Parks demonstrated through an experiment that the knockdown of AhR resulted in the downregulation of genes associated with cellular invasion and metastasis in TNBC.[24,25] There is mounting evidence that the recognizable inflamed TNBC phenotype is intrinsically linked to neoplasia. Additionally, constitutive AhR activity has been reported in multiple BC models of humans and rodents, complemented by recurring inflammatory elements. Hence AhR overexpression in TNBC cells presents a tractable therapeutic paradigm.[26] Genome-wide association studies combined with large-scale data obtained through multigene paneling have revealed PALB2, TP53, PTEN, STK11, BRCA1, and BRCA2 as the TNBC high-penetrance (HP) genes. These HP genes are susceptible to a multitude of mutations conferring the unique TNBC. The expression status of these biomarkers is of considerable prognostic significance in TNBC patients. Several studies have reported AhR knockdown to be intrinsically associated with cell-cycle arrest and apoptosis promotion in MD-MB-231 and MDA-MB-468 TNBC cell lines by modulating the molecular regulation of the key TNBC-responsive genes. Elson et al. claimed in their study that the small-molecule AhR inhibitors prevented malignant invasion in TNBC by restoring the transcriptional induction of several tumor-suppressive programs.[26] Hence inspired by the aforementioned scientific evidence and literature study, this computational work attempts to evaluate the antagonistic therapeutic effect of resveratrol on six HP TNBC receptors using various in silico techniques comprising thorough pharmacokinetic profiling, protein−ligand docking, and molecular dynamic simulations, in comparison to a standard TNBC chemotherapeutic drug, olaparib.[27]

https://doi.org/10.1021/acsomega.4c01317
ACS Omega 2024, 9, 30350−30363

2. MATERIALS AND METHODS

2.1. Ligand Retrieval and Preparation. The three-dimensional (3D) SDF structures of the ligands, viz., resveratrol (compound ID: 445154) and olaparib (compound ID: 23725625), were retrieved from the NCBI PubChem database available online.[28] Prior to molecular docking, Open Babel GUI was used to convert the SDF formats of both compounds into .mol[2] format.[29]

2.1.1. ADMET Parameters, Drug/Lead-Likeness, and Prediction. The physicochemical properties, ADMET, drug/lead-likeness, and bioavailability of our proposed ligand resveratrol were predicted using various online Web tools such as SwissADME, Molinspiration Cheminformatics, pkCSM, ADMETlab2.0, and ProTox-II.[30−33]

2.2. Protein Structure Retrieval and Preparation. The 3D crystal structures of the six HP receptors associated with TNBC, viz., PALB2 (PDB ID: 2W18), TP53 (PDB ID: 4MZI), PTEN (PDB ID: 1D5R), STK11 (PDB ID: 5WXN), BRCA1 (PDB ID: 1T15), and BRCA2 (PDB ID: 3EU7), were retrieved from Protein Data Bank database in PDB formats.[34] Validation of the structural conformations of the selected protein targets was performed using SAVES PROCECK version 6.0.[35] BIOVIA Discovery Studio was used to eliminate the water molecules, heteroatoms, and additional side chains from the receptor targets.[36] Following the incorporation of polar hydrogen, the PDB models of the proteins were subjected to tension minimization using Discovery Studio (BIOVIA) modeling packages, version 2021. The optimized receptor structures saved in the working directories further facilitate docking studies.

2.3. Receptor Binding-Site Prediction. Ahead of protein−ligand docking, the catalytic active sites present on the surface of the receptors along with their respective magnitudes of volume and area were determined using the online prediction server tool CASTp, version 3.0.[37] This was followed by uploading the refined models of the receptors to the online server. The sphere radius of the probe was sustained at 1.4 Å. Next, the binding sites possessing the highest volume and area dimensions were selected. The binding-site amino acids and their corresponding sequence IDs are recorded to facilitate grid optimization during docking.

2.4. Protein−Ligand Molecular Docking. Molecular docking estimating the binding potential of our studied compound, resveratrol, against the six HP proteins (HPPs), was performed using AutoDockTools (ADT) 1.5.6.[38] Thus, in ADT, the protein−ligand pairs were uploaded. The ligand torsion was calculated by using the root detection method. During docking, ligand torsion was configured to spin. In the meanwhile, the ligand aromaticity criteria were preset at 7.5.[39] Additionally, the receptor systems were optimized with hydrogen atoms and the incorporation of Kollman and Gasteiger charges. The initial docking optimizations were then preceded by saving the .pdbqt formats of the receptors and ligands. Subsequently, the grid box's dimensions, spacing, and placement were optimized to ensure that it encompassed the anticipated catalytic pocket of the receptors. AutoGrid was executed for grid map generation, followed by an AutoDock run. Lamarckian genetic algorithm was employed at default settings to investigate the active binding site possessing differential efficacy. Additionally, the typical molecular docking technique was employed, which consisted of 150 population runs and 50 GA runs, including an energy evaluation set with the highest evaluations of 25,000,000. The maximum generation size was preset to 27,000. Throughout the process, the protein models were held static, allowing flexible rotation of the ligand. The binding energies of the various protein−ligand conformations were further expressed in ascending order in terms of kcal/mol. Finally, the receptor−drug interactions were visualized and analyzed using the Discovery Studio visualizer and LIGPLOT$^+$ tool, version 2.25, respectively.[40]

2.5. Protein−Ligand Trajectory Analysis. Following docking studies, molecular dynamics simulations (MDS) were executed to assess the receptor−ligand structural equilibrium and to interpret the underlying transformations in the intrinsic dynamics of the best-docked receptor upon ligand binding. The protein-binding efficacy of our proposed lead resveratrol is compared in this study with reference to a clinically standardized TNBC inhibitor, olaparib. MDS was performed for both the best-docked receptor−resveratrol and receptor−olaparib pair exhaustively with GROMACS-2023.1 software package in Ubuntu version 22.04.2 LTS.[41] GROMOS96 54A7 was used as the force field for both the receptor−drug pairs. This is a basic force field designed for simulating molecules in explicit water where the dielectric screening effect of the aqueous environment is neglected. The force field is parameterized with a multiple-time-steeping scheme for a twin-range cutoff; hence, when used with a single-range cutoff, there might be variations from the intended values of physical properties (viz., temperature and density). The ligand topology was built by using ATB version 3.0. System solvation was carried out in a dodecahedral solvation box with crystallographic transferable intermolecular three-point molecules. Each constituent protein residue was maintained at physiological pH 7 with a constant periodic boundary implementation. This was followed by incorporation of charges K^+ and Cl^- ions following the Monte Carlo method of electrostatic neutralization.

The aforementioned pair of protein−ligand simulations proceeded in three major stages. The steepest descent algorithm was used for system geometry optimization, which constituted the first stage of the MDS. Following this, the system geometry underwent a two-stage equilibration involving 100 ps iterations at each stage. The foremost phase of equilibration maintains the *NVT* ensemble, following the Berendsen protocol. The Parrinello−Rahman barostat approach applied at 1 atm pressure and 303.15 K temperature retained at a constant *NPT* ensemble provided further guidance throughout the second system equilibration stage. This was followed by subjecting the two receptor−drug complexes to a 200 ns MDS each at a fixed *NPT* ensemble. The Particle-Mesh-Ewald algorithm was used to calculate the high-magnitude interactive forces to yield stable MD trajectories in the investigated receptor−drug complexes. The covalent interactive lengths were limited by implementing the LINCS technique of 2 fs integration. Additionally, applying the Verlet cutoff algorithm, many of the hydrophobic nonbonded interactions such as Coulomb and Jones interactions and van der Waal's forces were truncated at 10 Å.[42]

Multiple built-in tools of GROMACS were enabled to assess the MD trajectories of the protein−resveratrol (proposed combination) and protein−olaparib (control combination) complexes, to predict and compare the binding dynamics of resveratrol with respect to olaparib in terms of root-mean-square deviation (rmsd), root-mean-square fluctuations

https://doi.org/10.1021/acsomega.4c01317
ACS Omega 2024, 9, 30350−30363

(RMSF), radius of gyration (Rg), and solvent-accessible surface area (SASA) deviations. Additionally, the stability of both ligand-bound protein complexes was calculated in terms of hydrogen (H-bond) formation and total interaction energy. A total of 400 ns of MDS was produced. The various MD trajectories were visualized using VMD and images depicting the best conformational protein−ligand poses were generated. The multiple trajectory analyses performed thereby validate the curative superiority of the proposed dietary exogenous AhR agonist, resveratrol with regard to binding efficacy and conformational durability compared to olaparib toward the most optimally docked TNBC HPP target evaluated through this study.

2.6. Principal Component Analysis and Free-Energy Landscape Estimation. Principal component analysis (PCA) a commonly implemented critical approach is used for evaluating the dimensionality reduction of huge data sets. Additionally, PCA is a massively used method in MDS to depict the slow, functional motions of biomolecules. It was conducted in this study to evaluate the acquired conformational space and the deviations in the pattern of global atomic motion of our evaluated protein target while complexed with our proposed AhR agonist resveratrol and control drug olaparib. By diagonalizing and solvating the eigenvalues as well as the eigenvector for the covariance matrices, the principal components for both the drug-bound receptor pairs were estimated. The eigenvectors affirm directionality and eigenvalues demonstrate the magnitude of the atomic motion's strength, respectively.[43] Owing to the highly collective and strongly correlated motions to depict a sizable conformational region during the MD run, eigenvectors, viz., PC1 and PC2, were selected. The covariance matrix was calculated using the "gmx covar" tool of GROMACS. Additionally, the "gmx covar" was used to build and diagonalize the estimated covariance matrix. The "gmx_anaeig" utility was used for the computation of the eigenvectors associated with projection trajectories. Lastly, both of the eigenvectors of the receptor complexes bound to resveratrol and olaparib were plotted and examined.

Estimation of free-energy landscape (FEL) helps in improvised decoding of protein stability, folding, and conformational function. The GROMACS-enabled "gmx_sham" function was used to develop the FELs for both receptor-bound drug complexes. By computing the distribution probability of the two eigenvectors, PC1 and PC2, the FEL estimation was determined.

2.7. Binding Free Energy and Probability Density Function Analysis. In addition to molecular docking and dynamics simulation analysis, molecular mechanics/Poisson−Boltzmann surface area (MMPBSA) was calculated using the script-based "g_mmpbsa" tool for both the HPP−drug complexes to evaluate the thermodynamic stability of resveratrol and olaparib within the catalytic binding pockets of the receptors to assess the contribution of each binding pocket residue.[44] This approach demonstrates the mean of the two energetic terms, namely, solvation and potential energy, in vacuum. The molecular mechanics component is majorly based on van der Waal's interaction and an electrostatic component.[45] Additionally, the solvation energy is computed using polar solvation energy and nonpolar energy. Correspondingly, the polar solvation energy is calculated from the Poisson−Boltzmann equation, whereas the nonpolar solvation energy is calculated from SASA.[46] Followed by MMPBSA analysis, the binding energy data obtained were further used for plotting the probability density function (PDF) graph for both receptor-bound ligand complexes.

3. RESULTS

3.1. Physicochemical, ADMET, and Drug/Lead-Likeness Analysis. Analysis of the physicochemical and pharmacokinetic properties is a fundamental step in the drug discovery process that assists in determining the biological features of the proposed lead compound. The parameters of absorption, distribution, metabolism, excretion, and toxicity abbreviated as ADMET evaluate the pharmacokinetic profile of the proposed lead at the therapeutic dosage. Prior to receptor optimization, the physicochemical and pharmacokinetic (ADMET) properties and drug/lead-likeness of our proposed lead resveratrol were thus evaluated. The physicochemical properties calculated in terms of molecular weight, volume, topological surface area, octanol−water partition coefficient, rotatable bond number, hydrogen-bond acceptors (nON), hydrogen-bond donors (NOHNH), and molar refractivity were found to be within their permissible range of the respective parameters. Table S1 summarizes the various physicochemical properties of resveratrol. Tables S2 and S5 demonstrate the ADMET and drug/lead-likeness profile of the compound by using various online computational tools.

3.2. Receptor Retrieval and Preparation. The 3D crystalline PDB models of the TNBC HPPs selected through an exhaustive literature study were downloaded from the PDB database. The six HPPs comprising this study: PALB2, TP53, PTEN, STK11, BRCA1, and BRCA2, respectively, Figure S1. Table S6 depicts the resolution and sequence length of all 6 HPPs. Ramachandran plot evaluation revealed the six HPPs suitable for molecular docking as depicted in Table S7 and Figure S2. A receptor target is more accessible to a lead exhibiting the lowest binding energy. The crucial outcomes of the protein−ligand interactions have been further analyzed and discussed.

3.3. Catalytic Active Site Prediction of Receptors. The catalytically active regions within the receptor interfaces are frequently connected to conformational voids with a strong propensity to facilitate the binding of putative inhibitor compounds (Figure S3). Table S8 depicts the CASTp-identified binding residues of the TNBC HPPs evaluated in this study.

3.4. Analysis of Protein−Ligand Binding by Molecular Docking. ADTs determined the strength of binding interaction between the dietary AhR ligand, resveratrol, and the 6 TNBC receptors, viz., PTEN, TP53, PALB2, STK11, BRCA1, and BRCA2. The results revealed that resveratrol was antagonistically associated with the target receptors. A minimum distance of hydrogen bonds was considered in calculating the six pairs of HPP−resveratrol binding energies (kcal/mol). Table 1 depicts the scores of the binding energy and inhibition constants along with the interacting residues and distances between H bonds and residues involved in their formation. Hydrogen imparted the major binding attractive force in the HPP−resveratrol complexes, accounting for higher complex stability (Figure 1). The schematic representation of H-bond distances between the HPP−resveratrol pairs was generated using LigPlot, as represented in Figure S4. In addition to H bonds, the other interatomic forces of attraction present between the resveratrol-docked complexes are carbon−hydrogen (C−H) bonds, covalent and Pi−sulfur bonds, van der Waals force, Pi−ionic (cation/anion)

https://doi.org/10.1021/acsomega.4c01317
ACS Omega 2024, 9, 30350−30363

Table 1. HPP−Resveratrol Binding Energy Scores, Interacting Residues, Inhibition Constants, H-Bonded Residues, and Bond Distances Calculated by AutoDock

drug molecule	HPPs	scores of binding energies (kcal/mol)	interacting residues	H-bond residues	H-bonded distances (Å)	inhibition constant (μM)
resveratrol [$C_{14}H_{12}O_3$] (natural exogenous AhR antagonist)	PTEN	−5.78	Tyr16, Gln17, Glu18, Asp19, Gly20, Phe21, Asp22, Leu23, Asp24, Leu25, Thr26, Lys128, Glu157, Val158 and Arg161	Asp24, Gly20, Phe21 and Glu157	3.015, 2.893, 3.169 and 3.194	58.25
	TP53	−6.45	Val197, Glu198, Gly199, Asn200, Pro223, Glu224, Ser227, Tyr229, Thr230, Thr231, Ile232 and bTyr233	Glu198, Gly199, Tyr229, Ser227. Glu224	2.810, 3.073 2.565, 3.135 and 2.793	18.66
	PALB2	−7.9	Ser873, Ala874, Met875, Phe876, Ile922, Val923, Pro924, Val925, Pro926, Asp927, Val928, Tyr929, Leu931, Val932, Cys933, Gy1166 and Thr1167	Gly1166, Cys933, Asp927 and Val923	2.694, 2.745, 2.535, 2.667 and 3.088	1.61
	STK11	−5.45	Glu 35, Leu36, Asn38, Ser37, Glu40, Arg41, Ala109, Ser110, Gln111, Glu113 and Ser114	Trp228, Ser334, Asn224 and Met335	3.124, 2.910 and 2.863	100.75
	BRCA1	−5.65	Ser6, Thr7, Pro9, Ser1655, Gly1656 and Lys1702	Ser6 and Sep8	2.731 and 3.003	72.43
	BRCA2	−7.31	Val1123, Lys1124, Asp1125, His1126, Ala1128, Trp1140, Asp1141 and Trp1164	Csd1127 and Lys1124	2.674 and 2.951	4.41

interactive forces, and Pi−donor hydrogen bonds. The aforementioned findings thus further consolidate Huang-Zhao's notion, which postulates that hydrogen is not the only exclusive force of attraction that exists between the docked protein−ligand pairs.

Overall, the binding energy scores of resveratrol with the 6 HPPs were found to range between −5.45 and −7.9 kcal/mol. A more negative and lower score of binding energy indicates a stronger ligand-binding efficiency of the target receptors and an enhanced tendency toward stable formation of docked complexes. STK11 and PALB2 denoted the highest (−5.45 kcal/mol) and the least (−7.9 kcal/mol) scores of binding energies with resveratrol. Thus, as indicated from the docking results, PALB2 was demonstrated as a promising resveratrol target among the 6 frequently mutated TNBC receptors evaluated in this in silico investigation. Docking results further revealed that binding of resveratrol with PALB2 was stabilized by the formation of H bonds between the interacting residues Val923, Asp927, Cys933, and Gly1166 (Figure S4). Hence, as observed from docking analysis, since PALB2 was reported to fit best with resveratrol, the PALB2−resveratrol binding efficiency was further subjected to comparison with clinically standardized olaparib. To gain deeper insights into the binding mechanism of PALB2 with our proposed lead (resveratrol) in comparison to olaparib, evaluated as a controlled drug here, the study proceeded with detailed MDS analysis over 200 ns each for PALB2−resveratrol (proposed combination) and PALB2−olaparib (reference combination) complexes.

3.5. MDS Analysis. Over an estimated time series, proteins in a solution system migrate randomly and cause significant oscillations. Conformational unrest of target receptors caused by thermal energy amplification is anticipated to be the cause of these erratic movements. A thorough MD analysis helps to identify the important interacting amino acid residues that are hidden in the distinctive catalytic domains located on the surfaces of the receptor targets. Hence, a time-dependent molecular trajectory analysis spanning 200 ns is performed for the best-docked protein−ligand complex, PALB2−resveratrol with respect to olaparib. Using the GROMACS-2023.1 software package, a total of 400 ns of simulation was produced in this study.

3.5.1. Rmsd Estimation: Trajectory Analysis. rmsd provides an estimation regarding the conformational divergence from the beginning to the ultimate positional reference frame of the backbone atoms of the protein during the MD run. Higher structural stability usually corresponds to smaller deviations. In contrast, an elevated value of rmsd denotes higher conformational unrest in the receptor under investigation, indicating enhanced system destabilization. Additionally, a higher rmsd encountered in a particular protein−ligand complex indicates inadequate and mediocre ligand adaptation withheld in the receptor binding pocket.

Using the "gmx rmsd" command line, the rmsd of the 2 pairs of protein−ligand complexes is estimated, viz., PALB2−resveratrol and PALB2−olaparib, executed over 200 ns. From the plotted graph of PALB2-bound resveratrol and olaparib (Figure 2), it can be inferred that both the protein−ligand complexes converged around 110 ns, at about 0.75 nm, and proceeded with stable trajectories with no major fluctuation throughout the 200 ns MD run. The average rmsd value as depicted in Table S9, for PALB2 complexed with resveratrol and olaparib, is found to be 0.73 nm (depicted in black) and 0.83 nm (depicted in red), respectively. The lower

https://doi.org/10.1021/acsomega.4c01317
ACS Omega 2024, 9, 30350−30363

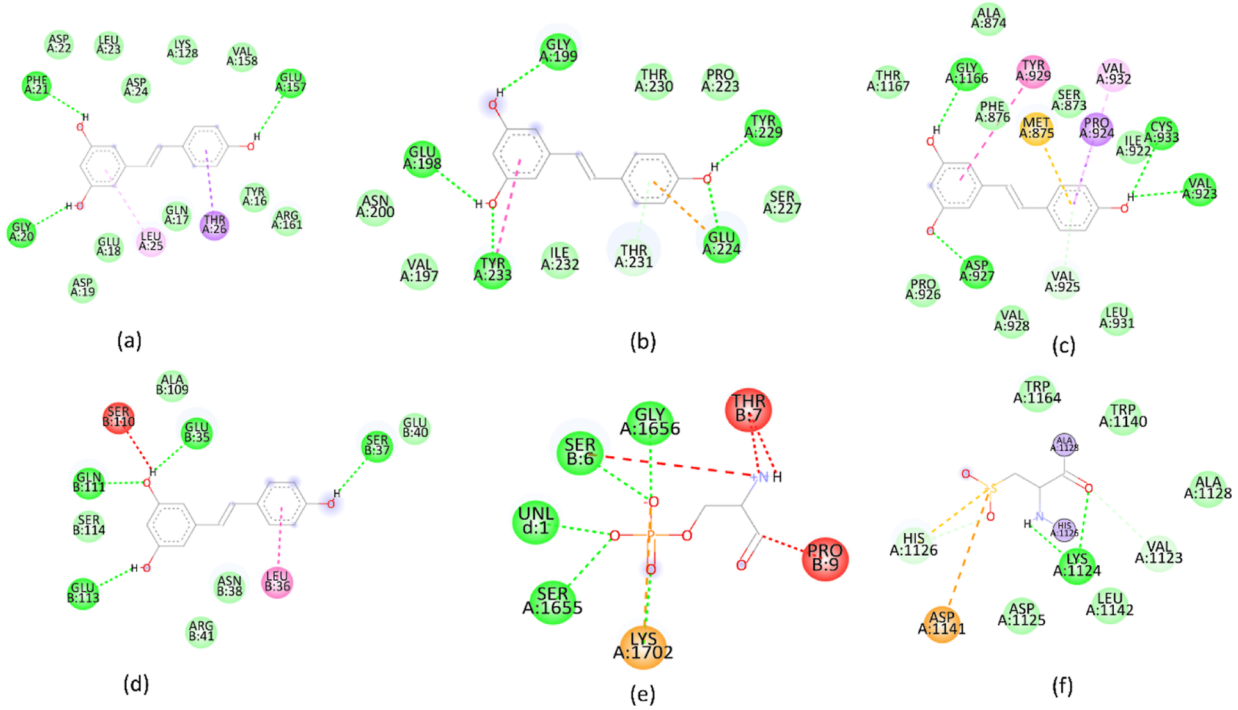

Figure 1. Schematic two-dimensional representation of the HPP−resveratrol complexes, green, light blue, and magenta, depicts the hydrogen, carbon−hydrogen, and pi−sigma bonds, respectively. (a) PTEN−resveratrol, (b) TP53−resveratrol, (c) PALB2−resveratrol, (d) STK11−resveratrol, (e) BRCA1−resveratrol, and (f) BRCA2−resveratrol.

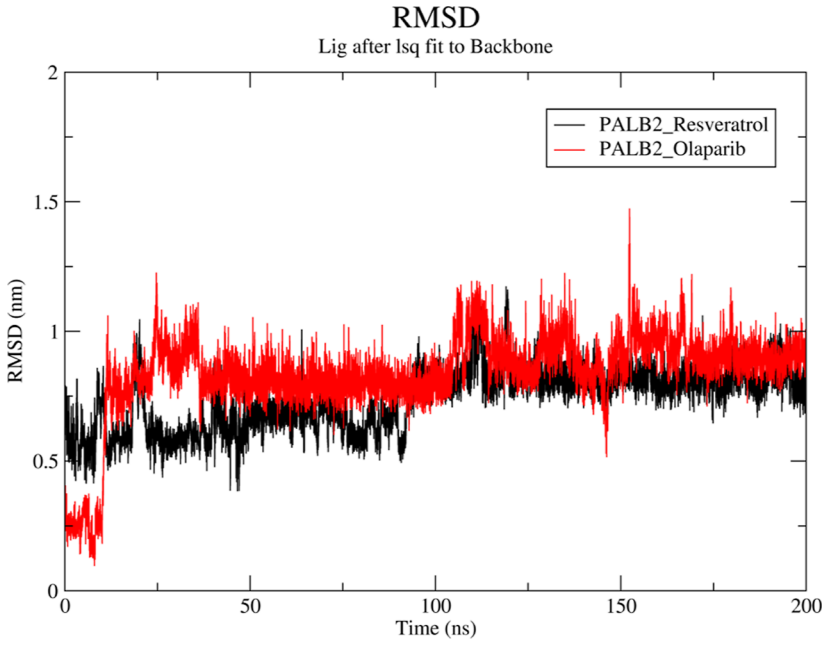

Figure 2. Rmsd of PALB2 complexed with resveratrol and olaparib generated over a 200 ns MDS.

average rmsd of our proposed ligand resveratrol with PALB2 thus suggests comparatively efficient binding dynamics, with enhanced conformational stability in comparison to olaparib complexed with the protein.

3.5.2. RMSF Estimation. The overall ligand-bound receptor backbone flexibility is estimated by RMSF. It calculates the residue-level variations to provide valuable insights concerning the impact of individual receptor residues involved in the dynamic conformational shift occurring in the complex. Thus a larger RMSF value indicates greater backbone fluctuations within the protein−ligand system. The command line "gmx rmsf" was therefore used to determine the residue-induced PALB2 flexibility when bound both with the proposed and control drugs estimated individually over 200 ns. From the graph plotted for both the pairs of ligand-bound PALB2 complexes (Figure 3), it is observed that the largest units of fluctuating residues were found between sequence lengths of 1050 and 1200 amino acid residues. Interestingly, maximum units of fluctuating residues were found in the PALB2−olaparib (highlighted in red) in a sequence length ranging

https://doi.org/10.1021/acsomega.4c01317
ACS Omega 2024, 9, 30350−30363

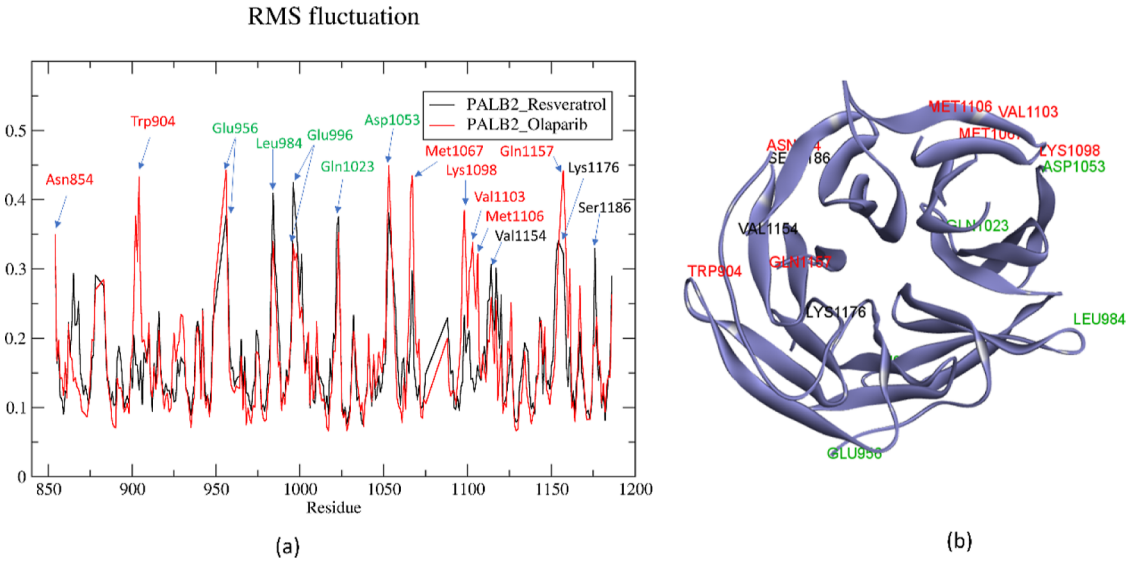

Figure 3. (a) RMSF of PALB2 complexed with resveratrol and olaparib generated over a 200 ns MDS. The common fluctuating residues in both complexes are highlighted in green. (b) Model of PALB2 with highlighted fluctuating amino acid residues.

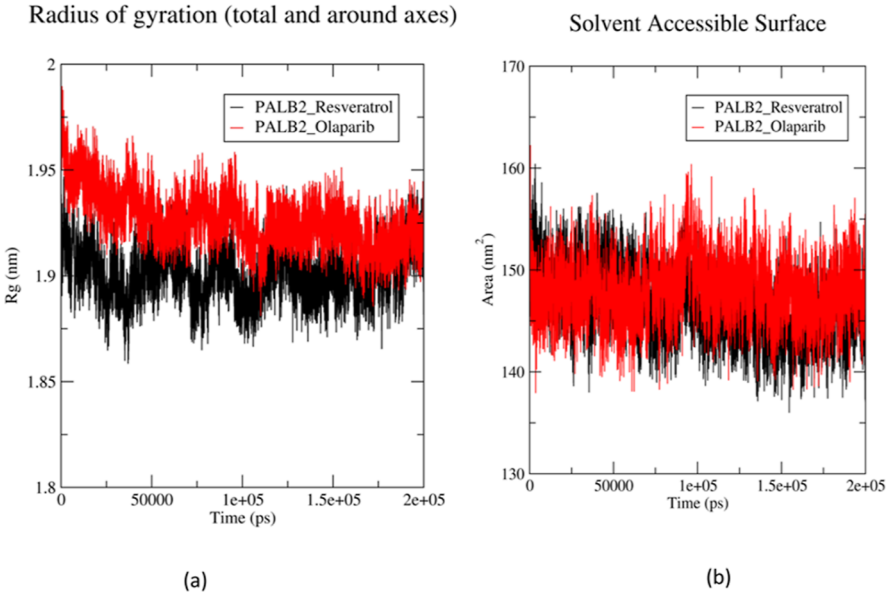

Figure 4. (a) Rg of PALB2−resveratrol and PALB2−olaparib calculated over a 200 ns MDS. (b) SASA of PALB2−resveratrol and PALB2−olaparib calculated over a 200 ns MDS.

between 1067 and 1176 amino acid residues, denoting a higher system instability compared to PALB2−resveratrol. The comparatively smaller number of high fluctuating peaks in the PALB2−resveratrol complex thus signifies a higher stability of the PALB2 backbone with highlighted reduced flexibility. The common fluctuating residues in both complexes (highlighted in green) ranging in sequence length between 956 and 1053 amino acid residues are Glu956, Leu984, Glu996, Gln1023, and Asp1053. The highest common fluctuating residue for both protein−ligand systems is Asp1053. The average RMSF value for the PALB2−resveratrol complex and PALB2−olaparib complex is 0.16 and 0.17 nm, respectively (Table S9). The lower mean RMSF of PALB2−resveratrol thus reflects the smaller numbers of higher peaks with fluctuations within the heterogeneous system, consequently resulting in a complex with enhanced dynamic stability when compared to the binding of PALB2 to olaparib.

3.5.3. Rg Estimation. Followed by the estimation of residue-level flexibility of the PALB2 backbone, we evaluated the impact of receptor compactness upon ligand binding. Rg is essentially indirectly correlated to the distance from the rotational axis. In a solvent system, the Rg estimation is a crucial parameter governing the conformational equilibrium and structural stability of the protein. Hence a higher Rg value corresponds to poor protein folding with less compactness. In this study, Rg was thus calculated to evaluate the effect of ligand binding, viz., resveratrol and olaparib, to estimate PALB2 compactness. The combined Rg graph (Figure 4a) depicts that both complexes proceeded with overlapping plots with no major fluctuations. The mean Rg calculated for the PALB2−resveratrol complex and PALB2−olaparib complex

https://doi.org/10.1021/acsomega.4c01317
ACS Omega 2024, 9, 30350−30363

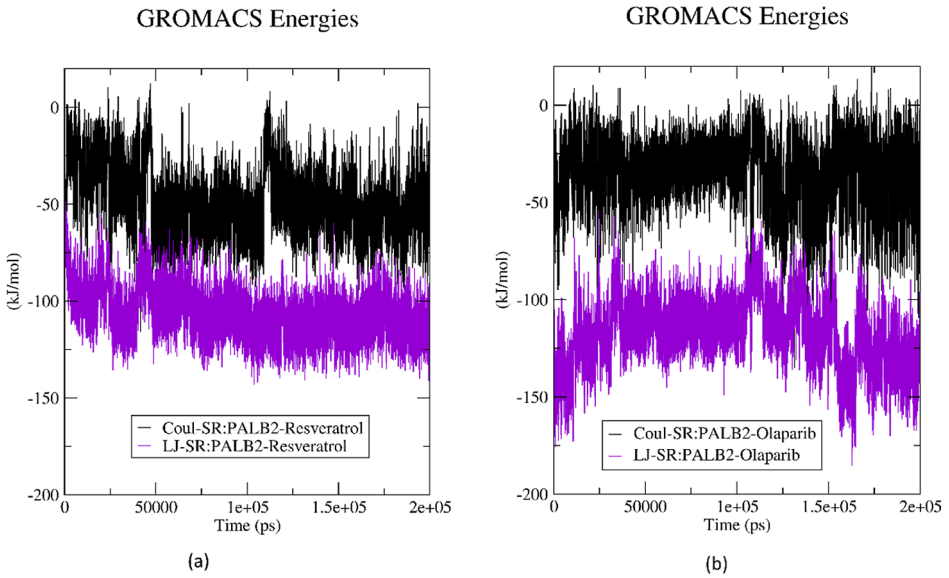

Figure 5. Total interaction energy calculated in terms of LJ-SR and Coul-SR energy for (a) PALB2−resveratrol and (b) PALB2−olaparib.

was 1.90 nm (depicted in black) and 1.92 nm (depicted in red), respectively (Table S9). The lower average Rg of resveratrol compared to olaparib when complexed with PALB2 thus suggests better binding conformational compactness of PALB2, when bound with our proposed ligand resveratrol than when bound to the control inhibitor, olaparib.

3.5.4. SASA Estimation. The receptor surface area that is available for solvent interaction is quantitatively estimated by SASA. Additionally, the SASA value deviance also confers a quantitative assessment concerning the exposure of the hydrophilic receptor residues to a polar system. It depicts a direct correlation with the Rg values of a complex. From the combined SASA graph plotted (Figure 4b), no significant differences in fluctuations were observed for both the complexes. However, the mean value of SASA for the PALB2−resveratrol complex was observed to be 146.68 nm^2 (depicted in black) and protein−olaparib was found to be 147.97 nm^2 (depicted in red), respectively (Table S9). PALB2 thus exhibits a higher affinity for binding with resveratrol than olaparib as justified by the complex's lower SASA value. Hence, the SASA estimation demonstrated that resveratrol provided PALB2 with reduced solvent exposure when compared to the control, olaparib, conferring receptor stability.

3.5.5. Hydrogen-Bond Calculation. Furthermore, the ultimate complex stability upon ligand ligation of the PALB2−drug combinations was evaluated through the estimation of H bonds. The formation of hydrogen bonds generally reflects the stability, binding specificity, and directionality of the drug-bound receptor systems. Owing to the stability it confers to the protein−ligand systems, H bonds are generally considered ligand-binding facilitators. From the plotted combined H-bond graph of the PALB2−resveratrol and PALB2−olaparib complex (Figure S5), it can be observed that hydrogen bonds calculated in the PALB2−resveratrol complex are comparatively higher ranging between 0 and 3 (depicted in black), in comparison to the number of H bonds calculated in the PALB2−olaparib complex ranging between 0 and 2 (depicted in red) in the 200 ns MDS. The average number of calculated H bonds in PALB2-bound resveratrol and olaparib is 0.51 and 0.17, respectively (Table S9), thereby denoting the stable binding dynamics of the PALB2−resveratrol system.

3.5.6. Estimation of Protein−Ligand Interaction Energy. The "gmx energy" command line was used to evaluate the contributions of the interacting residues of the protein for the calculation of the protein−ligand interaction energy. The sum of the short-range Lennard-Jones (LJ-SR) energy and Coulombic (Coul-SR) potential energy accounts for the total energy of the heterogeneous system.

For the PALB2−resveratrol complex (Figure 5a, Table S10), the LJ-SR and Coul-SR average energy was calculated to be −107.46 and −48.81 kJ/mol, respectively. Therefore, the protein−ligand interaction energy of the PALB2−resveratrol system was estimated to be −156.27 kJ/mol. On the other hand, the LJ-SR energy and the Coul-SR potential energy for the reference complex PALB2−olaparib (Figure 5b and Table S10) were observed to be −118.12 and −34.50 kJ/mol, respectively. Hence the protein−ligand interaction energy of the PALB2−olaparib complex was estimated to be −152.62 kJ/mol. A more negative interaction energy implies an enhanced equilibrium of the protein−ligand complexes. Hence the analysis of the protein−ligand interaction energy of both pairs of the PALB2 complex suggests stable binding conformation of the protein with resveratrol compared to olaparib. Thus, based on the comparative and exhaustive MDS analysis of the PALB2−resveratrol and PALB2−olaparib complex, it can be observed that the association of resveratrol to PALB2 induces a comparatively better conformational shift within the PALB2 catalytic domain than when bound to olaparib.

3.6. Principal Component Analysis. PCA evaluated the massive coordinated displacement of PALB2 while adhering to the ligands, viz., resveratrol and olaparib, throughout the 200 ns MDS. It is an unsupervised data reduction technique. The approach mainly focuses on the Cα atom fluctuations, leading to the diagonalization of the covariance matrices. Hence the coordinated motion of PALB2 during the 200 ns MD run is represented by the alpha-carbon atom displacement of the eigenvectors. The eigenvectors that were derived for both PALB2−resveratrol and PALB2−olaparib complexes are represented in Figure S6. PCA graphs were plotted using

https://doi.org/10.1021/acsomega.4c01317
ACS Omega 2024, 9, 30350−30363

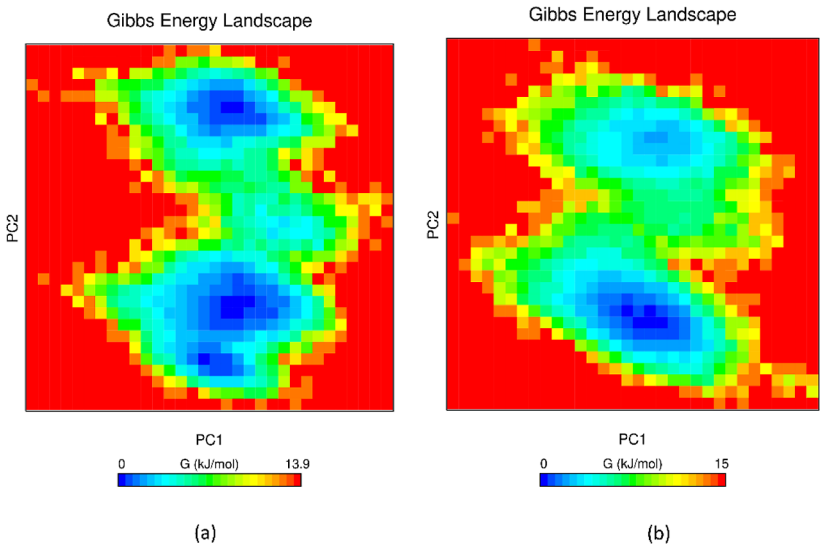

Figure 6. FEL models: (a) PALB2−resveratrol with three energy basins ranging between 0 and 13.9 kJ/mol and (b) PALB2−olaparib with two energy basins ranging between 0 and 15 kJ/mol.

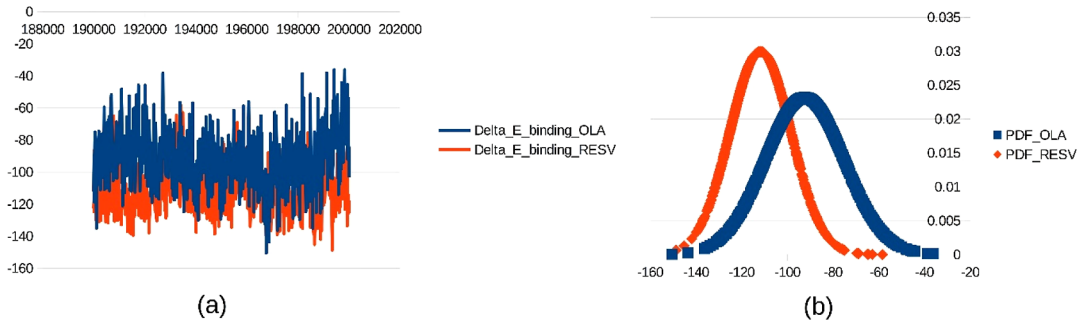

Figure 7. (a) Binding energy values calculated from MMPBSA analysis of PALB2−resveratrol and PALB2−olaparib complexes depicted in red and blue, respectively. (b) Combined PDF graph of PALB2-docked resveratrol (red) and olaparib (blue) complexes.

PC1 and PC2 as the two principal eigenvectors for both the PALB2−resveratrol and PALB2−olaparib complex. The PCA score plot exhibits distinct cluster formations. Both the PALB2−resveratrol and PALB2−olaparib clusters were found to be tightly overlapped, represented in black and red, respectively. Postdiagonalization, the trace of the PALB2−olaparib covariance matrix exhibited elevated motion amplitude raising its numerical value to 161.33 nm^2. Correspondingly, the covariance matrix trace of the PALB2−resveratrol complex exhibited well-defined clustered motion of lesser amplitude occupying a smaller area, with the covariance matrix value reduced to 152.27 nm^2. The energy distribution of the PALB2−olaparib cluster was comparatively wider than that of the proposed PALB2−resveratrol complex. The fluctuating nature of the PALB2−olaparib complex in the MD simulation could be the reason for its wider distribution in the score plot. Thus it can be inferred from the results obtained through PCA that the overall concerted movement of PALB2−resveratrol is restrained, as implied from its reduced covariance matrix value. In contrast, a larger motion amplitude with an elevated value of the covariance matrix is observed in the olaparib-bound PALB2 complex, which reflects enhanced structural flexibility of PALB2 with reduced stability, leading to the less compact accommodation of olaparib within the receptor's active site domain. The outcomes of PCA are thus in accordance with those of the aforementioned MD analyses including total interaction energy calculation, indicating that our test hit resveratrol is more compact and stable than olaparib in terms of PALB2 binding.

3.7. FEL Estimation. To differentiate among the distinct structural dispositions of the two PALB2−drug complexes following PCA, their corresponding FELs were generated. Using the MD trajectories corresponding to the ligand-bound protein complexes, FELs ascertain the directionality of the alpha-carbon atom fluctuations of both PALB2−resveratrol and PALB2−olaparib complexes. The FELs of PALB2 complexed with resveratrol and olaparib are depicted in Figure 6. Interestingly, three conformational energy basins (depicted in blue) are found to exist in the global energy minima of the PALB2−resveratrol complex, with energy values ranged between 0 and 13.9 kJ/mol. On the other hand, two distinct energy basins are found in the PALB2−olaparib complex with energy values ranging between 0 and 15 kJ/mol. The results infer that PALB2 upon binding to olaparib might experience a large conformational dynamic space and lesser thermodynamic stability. Contrastingly, upon binding to resveratrol, there is a decrease in the conformational space of the protein, and PALB2 adopts fairly stable conformations in the folding FELs. The conformations of free-energy minima are depicted in blue. Yellow and green signify metastable or intermediate protein conformations, whereas red indicates the high-energy state of the protein during simulations.

https://doi.org/10.1021/acsomega.4c01317
ACS Omega 2024, 9, 30350−30363

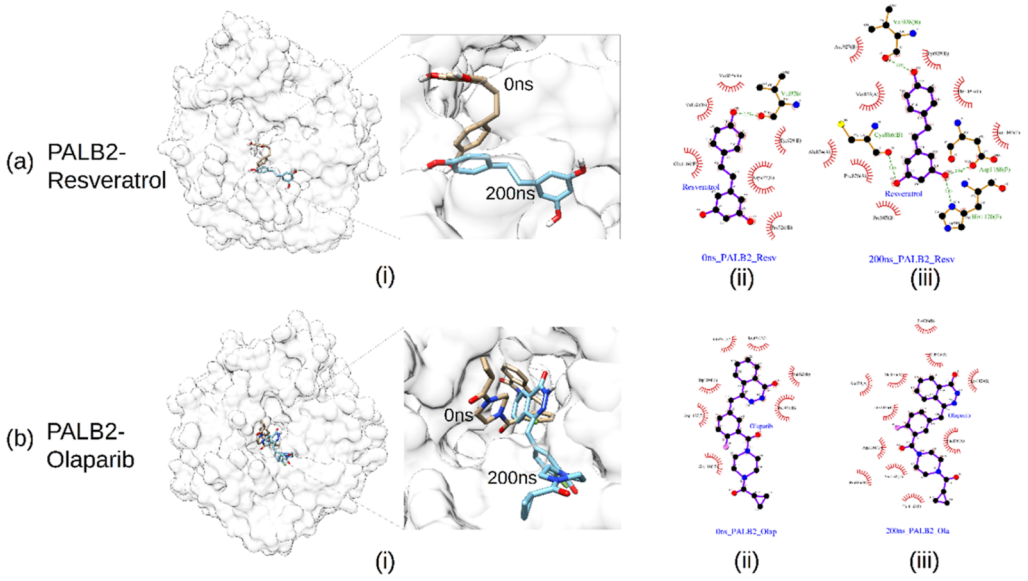

Figure 8. (a) PALB2−resveratrol (i) superimposed binding pose of 0 and 100 ns; (ii) PALB2−resveratrol interaction at 0 ns; (iii) PALB2−resveratrol interaction at 200 ns. (b) PALB2−olaparib (i) superimposed binding pose of 0 and 100 ns; (ii) PALB2−olaparib interaction at 0 ns; (iii) PALB2−olaparib interaction at 200 ns.

3.8. Estimation of Binding Free Energy and PDF Analysis. To comprehend the biophysical basis of resveratrol and olaparib's molecular interaction with PALB2, MMPBSA was computed. The binding free energies of the PALB2-docked resveratrol and olaparib complexes were calculated using the "g_mmpbsa" tool of GROMACS, each executed over 1002 frames equally distributed over the last 10 ns for both the PALB2−ligand trajectories. The detailed MMPBSA energy summary for the PALB2−resveratrol and PALB2−olaparib complexes is provided in Figures S9 and S10. The more negative the binding energy, the greater the binding affinity of the ligand to the receptor. Consequently, the binding energy of the PALB2−resveratrol complex was calculated to be −111.81 kJ/mol, whereas that of the PALB2−olaparib complex was −92.447 kJ/mol. Using the binding free-energy data obtained from MMPBSA, further, the PDF graph was plotted for both complexes. The free binding energy and the corresponding PDF graphs are depicted in Figure 7.

3.9. Postsimulation Analysis of Binding Pose and Interacting Residues. The "-dump" command of GROMACS was used to extract PDB files of both PALB2−resveratrol and PALB−olaparib complexes analyzed in this study, at a definite time interval of 50 ns between 0 and 200 ns. The analysis of different binding poses of both the studied ligands was performed using the PDBs of protein−ligand complexes extracted at a 50 ns time interval using the "-dump" command of GROMACS on the trajectory file (.xtc). The snapshots of the binding region and different poses of the ligand were generated by keeping the protein in the same orientation. Such an orientation helped to track the ligand motion in the protein pocket over time. It was observed that both the ligands are moving in the same binding pocket (Figure S11). Interaction analysis was performed on all the PDBs using LigPlot which shows that the number of interacting residues was found to be increasing with the progress of the simulation (Figure S12). The initial and last pose comparisons are shown in Figure 8. At 0 ns, resveratrol was interacting with 7 amino acids and was forming 1 hydrogen bond (Figure 8a), while at 200 ns, it was found to be interacting with 12 amino acids and forming 4 hydrogen bonds, depicting greater complex stability. Contrastingly, in the case of olaparib, (Figure 8b), only 7 amino acid residues were found to interact with PALB2 at 0 ns, which increased to 11 amino acid residues at 200 ns. The greater number of interacting residues and hydrogen-bond formation in resveratrol thus indicates that our proposed ligand has a better binding affinity toward PALB2 than olaparib.

4. DISCUSSION

Environmental toxins uplift the activity of the extremely conserved AhR, which on the other hand is antagonistically regulated by several natural exogenous ligands. Numerous genes and their products expressed in several tumors including BC have been shown to predict disease recurrence and OS, thereby often aiding in the selection of appropriate therapeutic regimens. Although these biomarkers including receptors may not be quantitative sensors of their functional activity or therapy outcome, upregulated AhR signaling was reported in both endocrine-responsive and independent instances of BC.[47] Depending on the hormonal status, the molecular subtypes of breast tumors impact the growth, spread, prognosis, and corresponding therapeutic response of the disease. Extreme molecular heterogeneity and a lack of pharmacologically pliable targets contribute to the clinical challenges of TNBC therapeutics. There is ample scientific evidence that correlates AhR expression with the upregulation of several genes associated with TNBC metastatic invasion and inflammation. The ability of AhR to induce epithelial−mesenchymal transition, rapid growth, invasion, and metastasis of breast neoplasm thus primarily establishes AhR's dominance in promoting mammary tumorigenesis.[11]

3D structural studies of the AhR receptor have aided in a better comprehension of the various conformational and molecular mechanisms of the receptor. While these studies enabled us to better understand AhR's DNA-binding domain, there remains much to comprehend regarding the ligand-binding PAS subunit of AhR. Despite the extreme similarity in domain homology among the various model organisms

https://doi.org/10.1021/acsomega.4c01317
ACS Omega 2024, 9, 30350−30363

studied, their individual PAS domains exhibited variations in their amino acid constitution contributing to interspecific variations in ligand specificity. Therefore, based on the antagonistic or agonistic nature of the ligands, their association with AhR produces various consequences upon binding. Diet is the primary way of exposure for humans and animals to both natural and synthetic AhR ligands.[48] Various natural metabolites are reported to modify the AhR pathway for numerous therapeutic and medicinal purposes.[21,49] The dietary exogenous ligands are majorly flavonoids, including polyphenols, isoflavones, flavonols, and flavones.

Obtained from plants, the stilbene derivative resveratrol produced via the phenylpropanoid metabolic route consists of two benzene rings held together by an isopropyl moiety in a double styrene bond.[17] The nonflavonoid stilbenoid polyphenol has several essential biochemical benefits of possessing favorable anticancer, antioxidant, anti-inflammatory, cardioprotective, antidiabetic, antimicrobial, and neuroprotective properties. Despite the well-known antitumor activities of resveratrol in several cancers such as colon cancer, colorectal cancer, multiple myelomas, ovarian cancer, prostate cancer, and hormone-receptive BCs, the role of resveratrol in the modulation of the aryl hydrocarbon signaling pathway in TNBC is less known.[50] Hence, in the current in silico investigation, resveratrol has been selected as the candidate lead to identify a suitable HP druggable biomarker among the six most commonly mutated receptors in TNBC. After the preliminary completion of computational screening of the physicochemical, pharmacokinetic, and medicinal properties, the binding affinity of the resveratrol with the 6 HPPs was determined. The stilbene polyphenol was mainly found to interact through the formation of H bonds with the 6 TNBC HP receptors.

Of the six receptor−resveratrol combinations evaluated, PALB2 exhibited excellent binding dynamics when ligated to the drug, accounting for a binding energy score of −7.9 kcal/mol. The protein which is 1186 amino acid residues in length in a genomic location of 16p.12.2 possesses a coiled-coil domain (9−42 residues in length), chromatin-associated motif (395−446), and a carboxyl (C) terminal WD40 domain (853−1186). The catalytic binding of the ligands generally takes place at the WD40 region of PALB2. As observed from molecular docking, Ser873, Ala874, Met875, Phe876, Ile922, Val923, Pro924, Val925, Pro926, Asp927, Val928, Tyr929, Leu931, Val932, Cys933, Gy1166, and Thr1167 are the main drug-binding residues of the protein. Among the interacting residues, Gly1166, Cys933, Asp927, and Val923 are the H-bonded residues providing stability to the ligand-bound PALB2.

Moreover, MDS was used to evaluate the structural flexibility and dynamic motion of PALB2 complexed with our test hit resveratrol with reference to the control chemotherapeutic inhibitor olaparib. The backbone rmsd of PALB2-bound resveratrol exhibited significantly fewer fluctuations with a consistent trajectory in comparison to that of the PALB2−olaparib complex. To facilitate a better understanding of the conformational perturbations dominating the key amino acid residues of the protein, RMSF was computed for PALB2 complexed with resveratrol and olaparib. Relatively milder structural variations accompanied by fewer deviating peaks were observed in the PALB2−resveratrol complex than in PALB2−olaparib. The Rg graph was plotted for PALB2 bound to resveratrol and olaparib for quantitative estimation governing receptor compactness. The average value of Rg is calculated to be 1.90 and 1.926 nm for the PALB2−resveratrol and PALB2−olaparib complex, respectively. The findings from the SASA calculation were also observed to be in accordance with the rmsd, RMSF, and Rg outcomes. The higher propensity of hydrogen bonds with comparatively less protein−ligand interaction energy implies greater stability of PALB2 when bound to resveratrol than to olaparib. Thus, the aforementioned results elucidate that resveratrol-bound PALB2 exhibited improved binding, enhanced compactness, and increased stability compared to the reference inhibitor olaparib. To assess the coordinated conformational movements of both PALB2 complexes, we performed PCA. The PALB2 complex bonded to olaparib showed greater flexibility and decreased compactness, demonstrating the superior conformation of PALB2−resveratrol binding, requiring approximately a minimum space of accommodation. Furthermore, FEL estimation indicated that resveratrol-bound PALB2 is more thermodynamically stable than olaparib.

Despite numerous developments in the comprehension of TNBC, the molecular anomalies underlying the hormone-deprived malignancy remain poorly understood.[51,52]

Irrespective of the hormonal status, the anticancer property of resveratrol BC includes inhibition of malignant cell invasion, proliferation, and induction of apoptosis. However, the primary antiproliferative activity of resveratrol is exerted through its capacity to prevent the activation and subsequent cytochrome P450 enzyme expression. Although the role of resveratrol as an exogenous AhR antagonist in TNBC is less explored, various in vitro studies reveal that in the BC cell lines, MDA-MB-231, BT-549, and T47D, resveratrol prevents oncogenic AhR-dependent transcription of the cytochrome P450 enzymes following nuclear translocation.[23,53] It restricts the AhR/AhR nuclear translocator (ARNT) complex from binding to its cognate DNA xenobiotic response elements (XRE) inside the nucleus. Additionally, in MCF-7, MDA-MB-231, and MCF-10A cells, evidence claims that dietary resveratrol dissociates the AhR/ARNT complex inside the nucleus to inhibit mRNA expression of cyp1a1 and cyp1b1 in TCDD-induced BC, following a mechanism similar to the other AhR antagonists. Phase-1 enzyme-activated PAH is believed to initiate carcinogenic processes through the conventional AhR-dependent signaling pathway. In a nutshell, PAH can attach to the AhR and aid in the latter's nuclear movement leading to the formation of the AhR/ARNT heterodimer. The hybrid complex subsequently adheres and activates the phase-I/II enzyme promoters that are driven by XRE, commencing the carcinogenesis cascade. It has been put forth that resveratrol can reduce this initial step by inhibiting AhR signaling.[50] The activated AhR pathway impairs ER-dependent transcription of the BRCA1 tumor suppressor gene in BC.[54] The addition of resveratrol was reported to suppress AhR-mediated promoter hyperphosphorylation, which induced epigenetic silencing of the BC tumor suppressor genes (TSGs) including BRCA-associated genes. Additionally, resveratrol restricts ER-independent regulation of the AhR pathway. Resveratrol-induced inhibition of CYP1B1 expression is also observed in both TNBC and ER-positive lines, thereby limiting the activation of the procarcinogen and suppressing the risk of tumorigenesis.

As a dysfunctional AhR-signaling pathway is frequently correlated to the mutational aberration of several BC TSGs, targeting the AhR-signaling pathway through biomarker-based

https://doi.org/10.1021/acsomega.4c01317
ACS Omega 2024, 9, 30350−30363

precision therapeutics may pave the way for a new treatment venture in the better therapeutic prognosis of TNBC. A mutation in the tumor suppressor PALB2 enhances the risk of hormone-refractory BC by 14% and thereby is recognized as a highly mutated HPP in TNBC.[55,56] Our study identifies PALB2 as a potential target of the AhR antagonist resveratrol. Inspired by the inference of our exhaustive in silico structural analysis, it can be postulated that by upregulating the reduced expression of the tumor suppressor, PALB2, resveratrol can repair the hyperactive AhR signaling in TNBC. Resveratrol-complexed PALB2 thereby in turn can prevent the conformational binding of the AhR XRE and the AhR−ARNT complex, inhibiting the subsequent activation of the cytochrome P450 enzymes and thus curbing the eventual onset of tumorigenesis. Hence, as far as BC-related precision therapeutics are concerned, PALB2 emerges in TNBC as a distinct druggable HP biomarker that exhibits enhanced binding dynamics when bound to our proposed AhR-signaling pathway inhibitor, resveratrol.

5. CONCLUSIONS

Constitutive expression of AhR signaling is often correlated with mutational aberrations of the hormone-refractory TNBC. The present computational investigation attempted to evaluate the medicinal curative efficacy of the natural AhR antagonist resveratrol in TNBC, by targeting the six frequently mutated HP genes of the disease. A preliminary in silico pharmacokinetic assessment revealed favorable physicochemical, ADMET (absorption, distribution, metabolism, excretion, and toxicity), medicinal, and drug-likeness parameters of resveratrol. On evaluating the binding interaction of resveratrol with the 6 TNBC HPPs, the results of molecular docking identified PALB2 as the most effective therapeutic target of our proposed hit. As PALB2 exhibited the highest binding affinity with resveratrol, the interaction dynamics of resveratrol−PALB2 were compared to a clinically approved TNBC chemotherapeutic inhibitor olaparib by an MDS study. During a 200 ns MDS, several MD trajectories were calculated for the two protein−drug combinations. The PALB2−resveratrol complex demonstrated less variations with minimal deviations, reflecting a more durable trajectory in comparison to PALB2−olaparib as reflected from their corresponding rmsd and RMSF graphs. Similarly, computation of Rg and SASA suggested the PALB2−resveratrol complex to be more compacted with a reduced inclination toward solvent interaction. Additionally, a higher propensity of H bonds in the PALB2−resveratrol complex and lower protein−ligand interaction energy depict higher stability and reduced flexibility of the resveratrol-docked complex in comparison to olaparib. Based on PCA and FEL estimations, the conformational space occupied by resveratrol is less than that of olaparib indicating enhanced thermodynamic stability and compactness of PALB2 upon binding of our proposed drug resveratrol than the standard inhibitor olaparib. Conclusively, the binding dynamics of resveratrol to the catalytic C terminal domain of PALB2 suggests a comparatively higher therapeutic and clinical efficacy of our proposed natural AhR antagonist resveratrol than olaparib through the alteration of AhR signaling. The comprehensive in silico analyses performed here thereby raise the reliability of potentiating PALB2 to be a distinct druggable HP receptor of the AhR antagonist resveratrol, an intriguing combination in TNBC precision therapeutics, thus awaiting additional in vitro studies.

■ ASSOCIATED CONTENT

Supporting Information

The Supporting Information is available free of charge at https://pubs.acs.org/doi/10.1021/acsomega.4c01317.

Related experimental details and results, including tables depicting the physicochemical properties, absorption scores, toxicity analysis results, and drug- and lead-like properties of resveratrol, resolution and sequence length and Ramachandran plot analysis of the 6 HPPs, ligand-binding residues present on the surface of the six TNBC HPPs, average rmsd, RMSF, Rg, SASA, and H-bond values of PALB2 complexed with resveratrol and olaparib, and the total of the LJ-SR and Coul-SR energy and figures depicting the crystal structures, Ramachandran plots, and ligand-binding pockets of the six TNBC HPPs, LigPlot analysis of the six complexes of HPP−resveratrol, and calculation of the H bond, 2D projection of trajectory, rmsd, total interaction energy, complete energy summary of MMPBSA analysis, snapshots, and interaction analysis of the PALB2−resveratrol and PALB2−olaparib complexes (PDF)

■ AUTHOR INFORMATION

Corresponding Author

Satarupa Banerjee − *School of BioSciences and Technology, Vellore Institute of Technology, Vellore 632014 Tamil Nadu, India*; orcid.org/0000-0002-0986-2796; Email: satarupa.banerjee@vit.ac.in, satarupabando@gmail.com

Authors

Prarthana Chatterjee − *School of BioSciences and Technology, Vellore Institute of Technology, Vellore 632014 Tamil Nadu, India*

Rohit Karn − *School of BioSciences and Technology, Vellore Institute of Technology, Vellore 632014 Tamil Nadu, India*

Arnold Emerson. I − *School of BioSciences and Technology, Vellore Institute of Technology, Vellore 632014 Tamil Nadu, India*

Complete contact information is available at: https://pubs.acs.org/10.1021/acsomega.4c01317

Author Contributions

†P.C. and R.K. contributed equally and shared first authors.

Notes

The authors declare no competing financial interest.

No financial assistance was associated with this work.

■ ACKNOWLEDGMENTS

The authors are sincerely grateful to the management of Vellore Institute of Technology, Vellore, Tamil Nadu, India, for providing the necessary infrastructure required for the development of this work.

■ REFERENCES

(1) Li, Y.; Zhang, H.; Merkher, Y.; Chen, L.; Liu, N.; Leonov, S.; Chen, Y. Recent advances in therapeutic strategies for triple-negative breast cancer. *J. Hematol. Oncol.* **2022**, *15*, 121.

(2) Sung, H.; Ferlay, J.; Siegel, R. L.; Laversanne, M.; Soerjomataram, I.; Jemal, A.; Bray, F. Global Cancer Statistics 2020: GLOBOCAN Estimates of Incidence and Mortality Worldwide

for 36 Cancers in 185 Countries. *Ca-Cancer J. Clin.* **2021**, *71* (3), 209−249.
(3) Turashvili, G.; Brogi, E. Tumor heterogeneity in breast cancer. *Front. Med.* **2017**, *4*, 227.
(4) Fukano, M.; Park, M.; Deblois, G. Metabolic flexibility is a determinant of breast cancer heterogeneity and progression. *Cancers* **2021**, *13* (18), 4699.
(5) Kvokačková, B.; Remšík, J.; Jolly, M. K.; Souček, K. Phenotypic heterogeneity of triple-negative breast cancer mediated by epithelial−mesenchymal plasticity. *Cancers* **2021**, *13* (9), 2188.
(6) Garrido-Castro, A. C.; Lin, N. U.; Polyak, K. Insights into molecular classifications of triple-negative breast cancer: Improving patient selection for treatment. *Cancer Discovery* **2019**, *9*, 176−198.
(7) Shimelis, H.; LaDuca, H.; Hu, C.; Hart, S. N.; Na, J.; Thomas, A.; Akinhanmi, M.; Moore, R. M.; Brauch, H.; Cox, A.; et al. Triple-negative breast cancer risk genes identified by multigene hereditary cancer panel testing. *J. Natl. Cancer Inst.* **2018**, *110* (8), 855−862.
(8) Recent advances in therapeutic strategies for triple-negative breast cancer.
(9) Hanieh, H. Toward understanding the role of aryl hydrocarbon receptor in the immune system: Current progress and future trends. *BioMed Res. Int.* **2014**, *2014*, 1−14.
(10) Sweeney, C.; Lazennec, G.; Vogel, C. F. A. Environmental exposure and the role of AhR in the tumor microenvironment of breast cancer. *Front. Pharmacol* **2022**, *13*, 1095289.
(11) Kay, J. E.; Cardona, B.; Rudel, R. A.; Vandenberg, L. N.; Soto, A. M.; Christiansen, S.; Birnbaum, L. S.; Fenton, S. E. Chemical Effects on Breast Development, Function, and Cancer Risk: Existing Knowledge and New Opportunities. *Curr. Environ. Health Rep.* **2022**, *9* (4), 535−562.
(12) Stockinger, B.; Meglio, P. D.; Gialitakis, M.; Duarte, J. H. The aryl hydrocarbon receptor: Multitasking in the immune system. *Annu. Rev. Immunol.* **2014**, *32*, 403−432.
(13) Murray, I. A.; Patterson, A. D.; Perdew, G. H. Aryl hydrocarbon receptor ligands in cancer: Friend and foe. *Nat. Rev. Cancer* **2014**, *14*, 801−814.
(14) Safe, S.; Zhang, L. The Role of the Aryl Hydrocarbon Receptor (AhR) and Its Ligands in Breast Cancer. *Cancers* **2022**, *14*, 5574.
(15) Chachay, V. S.; Kirkpatrick, C. M. J.; Hickman, I. J.; Ferguson, M.; Prins, J. B.; Martin, J. H. Resveratrol - pills to replace a healthy diet? *Br. J. Clin. Pharmacol.* **2011**, *72*, 27−38.
(16) Aggarwal, B. B.; Bhardwaj, A.; Aggarwal, R. S.; Seeram, N. P.; Shishodia, S.; Takada, Y. Role of resveratrol in prevention and therapy of cancer: Preclinical and clinical studies. *Anticancer Res.* **2004**, *24* (5A), 2783−2840.
(17) Gambini, J.; Inglés, M.; Olaso, G.; Lopez-Grueso, R.; Bonet-Costa, V.; Gimeno-Mallench, L.; Mas-Bargues, C.; Abdelaziz, K. M.; Gomez-Cabrera, M. C.; Vina, J.; et al. Properties of Resveratrol: In Vitro and In Vivo Studies about Metabolism, Bioavailability, and Biological Effects in Animal Models and Humans. *Oxid. Med. Cell. Longevity* **2015**, *2015*, 1−13.
(18) Casper, R. F.; Quesne, M.; Rogers, I. M.; Shirota, T.; Jolivet, A.; Milgrom, E.; et al. Resveratrol has antagonist activity on the aryl hydrocarbon receptor: Implications for prevention of dioxin toxicity. *Mol. Pharmacol.* **1999**, *56* (4), 784.
(19) Wong, P. S.; Li, W.; Vogel, C. F.; Matsumura, F. Characterization of MCF mammary epithelial cells overexpressing the Arylhydrocarbon receptor (AhR). *BMC Cancer* **2009**, *9* (1), 234.
(20) Bekki, K.; Vogel, H.; Li, W.; Ito, T.; Sweeney, C.; Haarmann-Stemmann, T.; et al. The aryl hydrocarbon receptor (AhR) mediates resistance to apoptosis induced in breast cancer cells. *Pestic. Biochem. Physiol.* **2015**, *120*, 5.
(21) Gearhart-Serna, L. M.; Davis, J. B.; Jolly, M. K.; Jayasundara, N.; Sauer, S. J.; Di Giulio, R. T.; Devi, G. R. A polycyclic aromatic hydrocarbon-enriched environmental chemical mixture enhances AhR, antiapoptotic signaling and a proliferative phenotype in breast cancer cells. *Carcinogenesis* **2020**, *41* (12), 1648−1659.
(22) Beedanagari, S. R.; Bebenek, I.; Bui, P.; Hankinson, O. Resveratrol inhibits dioxin-induced expression of human CYP1A1 and CYP1B1 by inhibiting recruitment of the aryl hydrocarbon receptor complex and RNA polymerase II to the regulatory regions of the corresponding genes. *Toxicol. Sci.* **2009**, *110* (1), 61−67.
(23) Chun, Y. J.; Kim, M. Y.; Guengerich, F. P. Resveratrol is a selective human cytochrome P450 1A1 inhibitor. *Biochem. Biophys. Res. Commun.* **1999**, *262* (1), 20−24.
(24) Goode, G. D.; Ballard, B. R.; Manning, H. C.; Freeman, M. L.; Kang, Y.; Eltom, S. E. Knockdown of aberrantly upregulated aryl hydrocarbon receptor reduces tumor growth and metastasis of MDA-MB-231 human breast cancer cell line. *Int. J. Cancer* **2013**, *133* (12), 2769−2780.
(25) Xue, P.; Fu, J.; Zhou, Y. The aryl hydrocarbon receptor and tumor immunity. *Front. Immunol.* **2018**, *9*, 286.
(26) Elson, D. J.; Nguyen, B. D.; Bernales, S.; Chakravarty, S.; Jang, H. S.; Korjeff, N. A.; Zhang, Y.; Wilferd, S. F.; Castro, D. J.; Plaisier, C. L.; et al. Induction of Aryl Hydrocarbon Receptor-Mediated Cancer Cell-Selective Apoptosis in Triple-Negative Breast Cancer Cells by a High-Affinity Benzimidazoisoquinoline. *ACS Pharmacol. Transl. Sci.* **2023**, *6* (7), 1028−1042. Jul 14
(27) Ellsworth, D. L.; Turner, C. E.; Ellsworth, R. E.; Li, C. J. A Review of the Hereditary Component of Triple Negative Breast Cancer: High- and Moderate-Penetrance Breast Cancer Genes, Low-Penetrance Loci, and the Role of Nontraditional Genetic Elements. *J. Oncol.* **2019**, *2019*, 1−10.
(28) Wang, Y.; Xiao, J.; Suzek, T. O.; Zhang, J.; Wang, J.; Bryant, S. H. PubChem: A public information system for analyzing bioactivities of small molecules. *Nucleic Acids Res.* **2009**, *37*, W623−W633.
(29) O'Boyle, N. M.; Banck, M.; James, C. A.; Morley, C.; Vandermeersch, T.; Hutchison, G. R. Open Babel: An Open chemical toolbox. *J. Cheminf.* **2011**, *3* (1), 33.
(30) Benet, L. Z.; Hosey, C. M.; Ursu, O.; Oprea, T. I. BDDCS, the Rule of 5 and drugability. *Adv. Drug Delivery Rev.* **2016**, *101*, 89−98.
(31) Banerjee, P.; Eckert, A. O.; Schrey, A. K.; Preissner, R. ProTox-II: A webserver for the prediction of toxicity of chemicals. *Nucleic Acids Res.* **2018**, *46* (W1), W257−W263.
(32) Dong, J.; Wang, N. N.; Yao, Z. J.; Zhang, L.; Cheng, Y.; Ouyang, D.; Lu, A. P.; Cao, D. S. Admetlab: A platform for systematic ADMET evaluation based on a comprehensively collected ADMET database. *J. Cheminf.* **2018**, *10* (1), 29.
(33) Verma, A. Lead finding from Phyllanthus debelis with hepatoprotective potentials. *Asian Pac. J. Trop. Biomed.* **2012**, *2* (3), S1735−S1737.
(34) Berman, H. M.; Westbrook, J.; Feng, Z.; Gilliland, G.; Bhat, T. N.; Weissig, H.; et al. The Protein Data Bank. *Nucleic Acids Res.* **2000**, *28*, 235−242.
(35) Laskowski, R. A.; Rullmann, J. A. C.; MacArthur, M. W.; Kaptein, R.; Thornton, J. M. AQUA and PROCHECK-NMR: Programs for checking the quality of protein structures solved by NMR. *J. Biomol. NMR* **1996**, *8* (4), 477.
(36) Discovery Studio. *Dassault Systemes BIOVIA, Discovery Studio Modelling Environment*, Release 4.5; Accelrys Software Inc, 2015.
(37) Tian, W.; Chen, C.; Lei, X.; Zhao, J.; Liang, J. CASTp 3.0: Computed atlas of surface topography of proteins. *Nucleic Acids Res.* **2018**, *46* (W1), W363−W367.
(38) Morris, G. M.; Huey, R.; Lindstrom, W.; Sanner, M. F.; Belew, R. K.; Goodsell, D. S.; Olson, A. J. AutoDock4 and AutoDockTools4: Automated docking with selective receptor flexibility. *J. Comput. Chem.* **2009**, *30* (16), 2785−2791.
(39) Trott, O.; Olson, A. J. AutoDock Vina: Improving the speed and accuracy of docking with a new scoring function, efficient optimization, and multithreading. *J. Comput. Chem.* **2009**, *31*, 455−461.
(40) Laskowski, R. A.; Swindells, M. B. LigPlot+: Multiple ligand-protein interaction diagrams for drug discovery. *J. Chem. Inf. Model.* **2011**, *51* (10), 2778−2786.
(41) Van Der Spoel, D.; Lindahl, E.; Hess, B.; Groenhof, G.; Mark, A. E.; Berendsen, H. J. C. GROMACS: Fast, flexible, and free. *J. Comput. Chem.* **2005**, *26*, 1701−1718.

https://doi.org/10.1021/acsomega.4c01317
ACS Omega 2024, 9, 30350−30363

(42) Páll, S.; Hess, B. A flexible algorithm for calculating pair interactions on SIMD architectures. *Comput. Phys. Commun.* **2013**, *184* (12), 2641−2650.
(43) Amadei, A.; Linssen, A. B. M.; Berendsen, H. J. C. Essential dynamics of proteins. *Proteins: Struct., Funct., Bioinf.* **1993**, *17* (4), 412−425.
(44) Kumari, R.; Kumar, R.; Consortium, O. S. D. D.; Lynn, A. g_mmpbsa—A GROMACS Tool for High-Throughput MM-PBSA Calculations. *J. Chem. Inf. Model.* **2014**, *54* (7), 1951.
(45) Maffucci, I.; Hu, X.; Fumagalli, V.; Contini, A. An efficient implementation of the Nwat-MMGBSA method to rescore docking results in medium-throughput virtual screenings. *Front Chem.* **2018**, *6*, 43.
(46) Al-Khafaji, K.; Taskin Tok, T. Molecular dynamics simulation, free energy landscape and binding free energy computations in exploration the anti-invasive activity of amygdalin against metastasis. *Comput. Methods Programs Biomed.* **2020**, *195*, 105660.
(47) Temchura, V. V.; Frericks, M.; Nacken, W.; Esser, C. Role of the aryl hydrocarbon receptor in thymocyte emigration in vivo. *Eur. J. Immunol.* **2005**, *35* (9), 2738−2747.
(48) Guyot, E.; Chevallier, A.; Barouki, R.; Coumoul, X. The AhR twist: Ligand-dependent AhR signaling and pharmaco-toxicological implications. *Drug Discovery Today* **2013**, *18*, 479−486.
(49) Tan, K. P.; Wang, B.; Yang, M.; Boutros, P. C.; MacAulay, J.; Xu, H.; Chuang, A. I.; Kosuge, K.; Yamamoto, M.; Takahashi, S.; et al. Aryl hydrocarbon receptor is a transcriptional activator of the human breast cancer resistance protein (BCRP/ABCG2). *Mol. Pharmacol.* **2010**, *78* (2), 175−185.
(50) Ko, J. H.; Sethi, G.; Um, J. Y.; Shanmugam, M. K.; Arfuso, F.; Kumar, A. P.; Bishayee, A.; Ahn, K. S. The role of resveratrol in cancer therapy. *Int. J. Mol. Sci.* **2017**, *18*, 2589.
(51) Perreault, A. A.; Sprunger, D. M.; Venters, B. J. Epigenetic and transcriptional profiling of triple negative breast cancer. *Sci. Data* **2019**, *6*, 190033.
(52) Sarmiento-Salinas, F. L.; Delgado-Magallón, A.; Montes-Alvarado, J. B.; Ramírez-Ramírez, D.; Flores-Alonso, J. C.; Cortés-Hernández, P.; Reyes-Leyva, J.; Herrera-Camacho, I.; Anaya-Ruiz, M.; Pelayo, R.; et al. Breast cancer subtypes present a differential production of reactive oxygen species (ROS) and susceptibility to antioxidant treatment. *Front. Oncol.* **2019**, *9*, 480.
(53) Tomé-Carneiro, J.; Larrosa, M.; González-Sarrías, A.; Tomás-Barberán, F.; García-Conesa, M.; Espín, J. Resveratrol and Clinical Trials: The Crossroad from In Vitro Studies to Human Evidence. *Curr. Pharm. Des.* **2013**, *19* (34), 6064−6093.
(54) M Hall, J. The Aryl-hydrocarbon Receptor (AhR) as a Therapeutic Target in Human Breast Cancer. *J. Steroids Horm. Sci.* **2013**, *05* (03), 1.
(55) Laraqui, A.; Cavaillé, M.; Uhrhammer, N.; ElBiad, O.; Bidet, Y.; El Rhaffouli, H.; et al. Identification of a novel pathogenic variant in PALB2 and BARD1 genes by a multigene sequencing panel in triple negative breast cancer in Morocco. *J. Genomics* **2021**, *9*, 43.
(56) Sun, X.; Wang, M.; Wang, M.; Yao, L.; Li, X.; Dong, H.; Li, M.; Sun, T.; Liu, X.; Liu, Y. Role of Proton-Coupled Monocarboxylate Transporters in Cancer: From Metabolic Crosstalk to Therapeutic Potential. *Front. Cell Dev. Biol.* **2020**, *8*, 651.

https://doi.org/10.1021/acsomega.4c01317
ACS Omega 2024, 9, 30350−30363